Near-Ideal RF Upconverters

N. Vasudev and Oliver M. Collins, *Fellow, IEEE*

***Abstract*—This paper presents experimental results on the application of a new quadrature modulator compensator, which allows existing quadrature modulators to achieve near-ideal RF upconversion over a wide bandwidth. A test setup using an arbitrary waveform generator and a spectrum analyzer shows that over 70 dB of spurious-free dynamic range may be obtained over a bandwidth of 1.2 MHz using an off-the-shelf Mini Circuits in-phase/quadrature modulator operating at 895 MHz. A conventional compensator provides only 45 dB of sideband suppression in the same experimental setup.**

***Index Terms*—Complex filter, direct upconversion, frequency dependent compensation, quadrature modulator.**

I. Introduction

DIRECT-CONVERSION transmitters are gaining popularity because of their compact implementation. However, they have problems [1], [2] that do not exist in their competing architecture, i.e., the superheterodyne. The weak link in a direct-conversion transmitter is the quadrature modulator. A quadrature modulator takes baseband in-phase/quadrature (IQ) signals and translates them into a single real signal at RF. Unfortunately, there are imperfections in the quadrature modulator that result in an unwanted image signal (sideband leakage) and a residual tone at the carrier (carrier leakage). These imperfections limit the performance of many communication systems, e.g., in frequency-division multiplex systems with baseband tuning (i.e., software radio), the unwanted image signal appears as interference in an adjacent channel. This paper mitigates these nonidealities by applying a new frequency-dependent compensator [3] to an existing quadrature modulator. The results from a test setup based on an off-the-shelf Mini Circuits, Brooklyn, NY, IQ modulator show that the imperfections can be reduced to below the -70-dBc level by using the new compensator, while conventional compensators reduce the imperfections to only the -45-dBc level.

Quadrature modulators are usually built with two mixers, a 0° power combiner and a 90° power splitter. Unfortunately, most 90° power splitters do not generate signals that are exactly 90° out-of-phase. This error is shown as ϕ in Fig. 1. There is also a gain imbalance between the two arms represented by k in Fig. 1. Frequency-dependent effects also occur in the quadrature modulator, as represented by the filters in the model [3]. (The filters in between the mixers and the summer in Fig. 1 are the new additions to the model that make the improved baseband correction capability reported in this paper possible.) These imperfections cause sideband leakage, which is observed at the image frequency. For example, if a single complex sinusoid is transmitted on the I and Q arms, multiple tones are observed at the output of the quadrature modulator. The desired tone occurs at the complex sinusoid frequency and an unwanted tone occurs at its image frequency (as shown in Fig. 1). Carrier leakage, i.e., a tone at the carrier frequency, is also a common imperfection observed in quadrature modulators. Commercial quadrature modulators have other nonidealities, apart from these gross effects, e.g., baseband nonlinearity, which become significant only when the gross effects described above are removed.

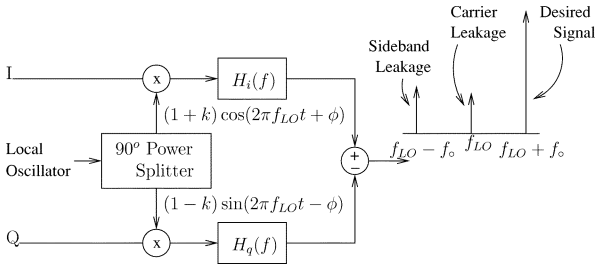

Fig. 1. Model of a quadrature modulator.

Much research effort has been devoted to designing 90° power splitters with low phase error [4], [5] for quadrature modulators. Baseband predistortion techniques [3], [6], [7] that compensate for nonidealities in the quadrature modulator using digital processing relax the requirements on the analog circuitry of the quadrature modulator. Faulkner *et al*. [6] suggests a frequency-independent compensator that obtains small gains in spurious-free dynamic range when used in wide-bandwidth upconverters. Leyonhjelm [7] considers the mismatch in the reconstruction filters, but ignores frequency-dependent effects inside the quadrature modulator itself. He suggests the use of one frequency-independent compensator for each channel in a frequency-division multiplex system. This paper describes an application of the frequency-dependent compensator and the iterative measurement algorithm suggested in [3]. This compensator uses a complex filter to remove the sideband leakage component and a complex dc value to remove the carrier leakage.

II. Frequency-Dependent Compensator

The frequency-dependent compensator is shown as part of a complete RF upconverter in Fig. 2. The complex sideband cancellation filter $H_c(f)$ and the equalization filter $H_e(f)$ compensate for the frequency-dependent sideband leakage. The single complex parameter C_p compensates for the carrier leakage. The real and imaginary outputs of the compensator are sent to the I and Q inputs of the quadrature modulator. In other words, the composition of the imperfect quadrature modulator and the

Manuscript received July 29, 2001.

N. Vasudev is with Stryker Endoscopy, San Jose, CA 95138 USA (e-mail: vnambaka@nd.edu).

O. M. Collins is with the Department of Electrical Engineering, University of Notre Dame, Notre Dame, IN 46556 USA

Digital Object Identifier 10.1109/TMTT.2002.804507

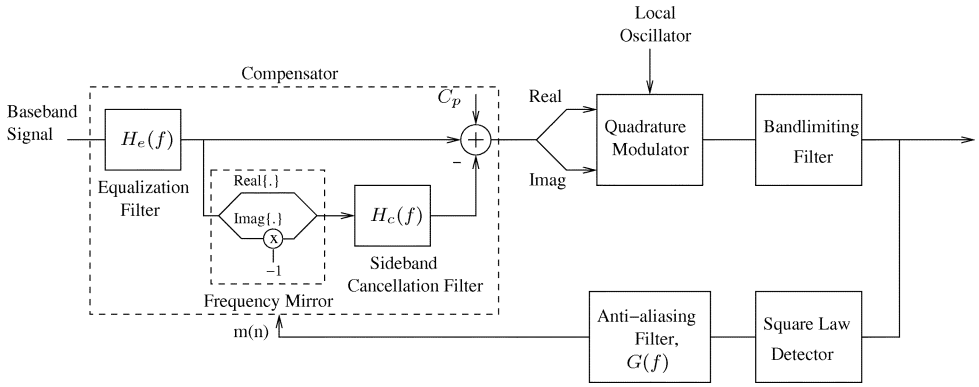

Fig. 2. Transmission system with compensator.

compensator is equivalent to an ideal quadrature modulator. The equalization filter $H_e(f)$ has only a second-order effect [3] and can be ignored in most cases. In systems that require a frequency-independent signal path, e.g., those attempting some sort of linearization of a power amplifier [8], $H_e(f)$ may be used to equalize the forward signal path. $H_e(f)$ can be measured using the techniques suggested in [9] and [10], but it is not discussed further in this paper. $H_c(f)$, of course, always has to be measured.

There are many possible feedback mechanisms to measure the quadrature modulator; however, a square-law detector is by far the simplest and cheapest (see Fig. 2). The measurement algorithm applied in Section III uses a square-law detector in the feedback and employs a test signal.

III. Measurement Algorithm

If a sine wave at frequency f_0 is applied to the quadrature modulator, multiple tones are observed at its output (see Fig. 1). The dominant tones are the desired sinusoid and those due to sideband and carrier leakage. The power detector beats the desired sinusoid with the tones resulting from the sideband and the carrier leakage to generate sinusoids at frequencies $2f_0$ and f_0, respectively. The tone at $2f_0$ is proportional to the unwanted sideband and the tone at f_0 is proportional to the carrier feedthrough. When the feedback filter $G(f)$ is not known precisely, there is a small error in the observed amplitude and phase. Synchronous detection of the tones at $2f_0$ and f_0 is the key to measurement of the compensation parameters $H_c(f)$ and C_p.

The sideband cancellation filter $H_c(f)$ is obtained by measuring the complex compensation parameters $H_c(f_i)$ at a small number of frequency points f_i (i represents the index) in the operating signal bandwidth. The response $H_c(f_i)$ at each frequency is found by transmitting a complex sinusoid at that frequency and nulling out the sinusoid at the image frequency by observing the amplitude and phase of the sinusoid at $2f_i$ in the feedback. The cancellation is performed by adding a complex sinusoid at the image frequency with the same magnitude as the unwanted image and and 180° out-of-phase. Employing this procedure iteratively makes the algorithm robust to feedback path errors. The magnitude and phase of the sinusoid at $2f_i$ are obtained using a synchronous detector and are represented by $(\alpha + j\beta)$ in (1) as follows:

$$H_c(f_i)|_{\text{present}} = H_c(f_i)|_{\text{previous}} + (\alpha + j\beta). \tag{1}$$

Similarly, C_p is obtained by nulling out the residual carrier by observing the amplitude and phase of the sinusoid at f_i in the feedback signal while transmitting a complex sinusoid at that frequency. The cancellation, in this case, is obtained by generating a negative dc offset. Equation (2) shows the cumulative dc offset that is subtracted from the transmitted signal. The magnitude and phase of the sinusoid at f_i are obtained using a synchronous detector and are represented by $(\eta + j\gamma)$. As in the case of the image sinusoid measurement, an iterative algorithm is required in the presence of feedback path errors. The carrier compensation parameter C_p is independent of the baseband signal frequency f_i; hence, this measurement need not be repeated for each f_i.

$$C_p|_{\text{present}} = C_p|_{\text{previous}} + (\eta + j\gamma). \tag{2}$$

The synchronous detection of the sinusoids at f_i and $2f_i$ are shown in (3) and (4), respectively. The sampled feedback signal is represented as $m(n)$ and T is the sampling period. The scaling factor g and delay τ represent the gain and delay compensation of the feedback signal chain. N and M represent the duration of matched filtering.

$$\alpha + j\beta = g \cdot \sum_{n=0}^{N-1} m(n) e^{2\pi 2 f_i (n-\tau) T} \tag{3}$$

$$\eta + j\gamma = g \cdot \sum_{n=0}^{M-1} m(n) e^{2\pi f_i (n-\tau) T}. \tag{4}$$

The computations in (3) and (4) may also be performed as a fast Fourier transform (FFT), but the sign of the phase term has to be changed appropriately. Techniques such as windowing can be applied when the duration of the matched filter does not include an integral number of periods of the sinusoids. Windowing may also be profitably applied when the transmission signal path and the feedback path circuitry have a small asynchronism, e.g., asynchronous sampling clocks.

The observed sinusoids at f_i and $2f_i$ at the detector output come not only from carrier leakage and the unwanted sideband, respectively, but also from second- and third-order baseband

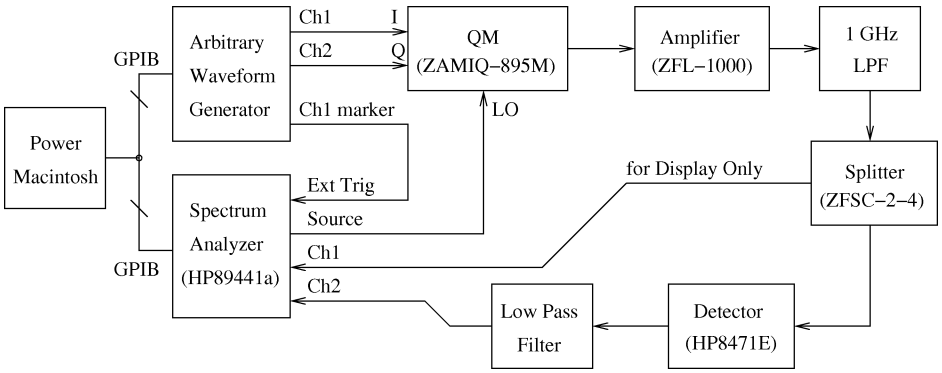

Fig. 3. PC-based measurement setup.

nonlinearities, respectively, of the mixers within the quadrature modulator. Hence, the residual carrier and sideband can be cancelled only to the level of the spurious signals caused by mixer nonlinearity. Also, the power detector is not an ideal square-law device. Its higher order terms generate spurious signals at $2f_i$ at the output when the carrier leakage is large. Hence, the measurement algorithms for $H_c(f_i)$ and C_p should be implemented in parallel. Fortunately, this is also the most efficient procedure since they both use the same sinusoidal excitation.

Even though the iterative algorithm represented by (1) and (2) is robust against small feedback path errors, the major component of the phase error, i.e., the group delay of the feedback path, will have to be measured at least once when the product is made and may be profitably measured in real time if temperature stability is poor. Section IV describes the group-delay measurement technique used for the experiments presented in this paper, and describes the effect of residual errors in the feedback path on the performance of the sideband and carrier nulling procedures.

IV. Feedback Path Uncertainties

The group delay of the feedback path can be obtained by measuring the phase difference between two closely spaced sinusoids. In this case, a sinusoidal excitation signal at frequency f_0 is generated at the output of the power detector [at the input to $G(f)$] by beating two tones at $f_{\rm LO} \pm (f_0/2)$ at the output of the quadrature modulator ($f_{\rm LO}$ is the quadrature modulator's local oscillator (LO) frequency). This can be easily achieved by transmitting a sinusoid at frequency $f_0/2$ on one of the arms of the quadrature modulator and silence on the other. (Since only one mixer is excited, the first-order quadrature-modulator imperfections, i.e., k and ϕ, will not have any effect on this group delay measurement.) The phase of the sinusoid at the output of the antialiasing filter $G(f)$ is measured by using a matched filter [similar to that shown in (3) and (4)]. The frequency of the sinusoid at the input to the quadrature modulator is perturbed by δf and the phase of the sinusoid at the output of $G(f)$ is recorded using a matched filter at the frequency $f_0 + 2\delta f$. If the difference in the phases is ϕ, the group delay of the feedback path is $(\phi)/(4\pi\delta f)$. The sample delay is $\tau = (\phi)/(4\pi T\delta f)$, where T is the sampling frequency. The frequency offset δf is chosen to be small enough so that the phase error is less than 2π, and large enough for local deviations in phase to be negligible. The scale factor g is obtained as the reciprocal of the magnitude of the matched filter output at f_0.

The measurements described above will naturally have some error associated with them. These may be because of the measurement error or may be caused by drift since the measurement was actually made. If k_g and θ represent the residual gain and phase uncertainties, respectively, in the feedback path at the frequency of interest, the algorithm simply observes a sinusoid that is distorted by k_g and θ. If the initial sinusoid is represented as a unit vector, the residual sinusoid after the cancellation is represented by the vector distance between the unit vector and a vector of magnitude k_g and phase θ. The magnitude of the residual sinusoid will be lower than the initial sinusoid only if this vector distance $|1 - k_g e^{j\theta}|$ is less than unity. Simplification using basic trigonometry gives the convergence criterion as $0 < k_g < 2\cos(\theta)$, i.e., θ must be less than 90° for the algorithm to converge and, for θ close to 90°, k_g must be small (close to zero) in order to achieve convergence.

The feedback uncertainties k_g and θ also affect the integration time required by the matched filter (N and M of (3) and (4), respectively). Specifically, [3] shows that the steady-state power in the residual sideband and carrier is equal to the detector noise power at the output of the respective matched filters multiplied by $(k_g)/(2\cos(\theta) - k_g)$. A small value of k_g reduces the steady-state power by averaging over many matched-filter measurements. Further, a small value of k_g allows a large range for uncertainty in the phase θ, while ensuring convergence. Thus, there is no need to measure k_g accurately since it can be deliberately biased to a small value.

V. Measurement Setup

The test setup consists of a personal computer (PC) networked with a Sony/Tektronix arbitrary waveform generator (AWG) and an Hewlett-Packard (HP) vector signal analyzer (VSA), as shown in Fig. 3. The I and Q signal generation is performed by the AWG, while the VSA performs the feedback measurement. The compensation is implemented by the PC. The quadrature modulator under test is an off-the-shelf Mini Circuits ZAMIQ-895M, which is specified for operation in the carrier frequency range of 868–895 MHz and provides typical sideband and carrier levels of −40 dBc. The low-pass filter following the quadrature modulator attenuates the higher frequency components that result from modulation of the

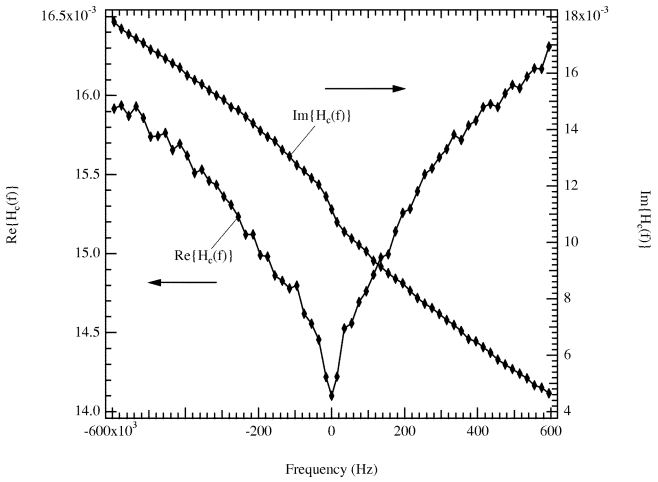

Fig. 4. $H_c(f)$ for 1.2-MHz bandwidth at 895 MHz.

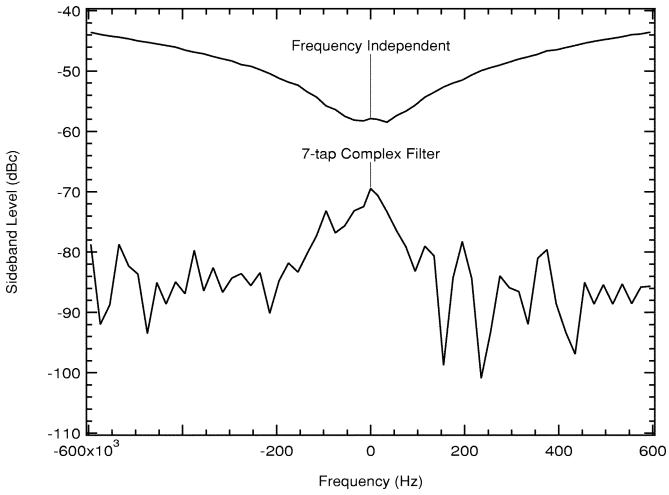

Fig. 5. Sideband attenuation obtained using a complex cancellation filter.

baseband signal with harmonics of the LO. In this experiment, the filter employs two Mini Circuits SLP-1000s to obtain 60–70-dB attenuation at the second harmonic. The splitter, i.e., Mini Circuits ZFSC-2-4, is chosen to have a flat frequency response over the frequency of operation. The detector is a Schottky diode HP8471E from Agilent Technologies, Palo Alto, CA. The noise voltage at the output of the detector is 10 nV/rtHz and a residual sideband of -70 dBc produces a 50-$\mathrm{nV_{rms}}$ signal.

As described in Section IV, the second and third harmonics generated at the baseband inputs to the quadrature modulator restrict the carrier and sideband cancellation, respectively. However, since the second- and third-order harmonics themselves contribute to the in-band distortion, they have to be reduced anyway. In other words, the power detector measurement technique does not impose any additional linearity constraints on the mixer. In this measurement setup, the baseband signal level is chosen such that the second and third harmonics are at least 70 dB below the desired signal so that the carrier and sideband may be suppressed to at least 70 dB below the desired signal. The carrier level for this measurement setup was $+10$ dBm, and the second harmonic level was of the order of -70 dBc, while the third harmonic was lower than -80 dBc.

VI. Sideband Compensation

Fig. 4 shows the sideband cancellation filter $H_c(f)$ over a bandwidth of 1.2 MHz at 895 MHz. The cancellation filter is measured at 60 points in the frequency range $(-595, 595)$ kHz spaced 20-kHz apart. Sideband levels of up to -80 dBc are obtained at the frequency points where the cancellation filter is measured. The response at 0 Hz is obtained by interpolation. The diamonds (except at 0 Hz) indicate the frequencies at which the measurement is made. The asymmetry in the response is due to a nontrivial asymmetric frequency response between the mixers and the summer in the quadrature modulator (as shown in Fig. 1). Fig. 5 shows that the sideband level obtained on the setup using a conventional frequency-independent compensator is as high as approximately -45 dBc (a gain of only approximately 5 dB from typical values of the raw modulator), while a

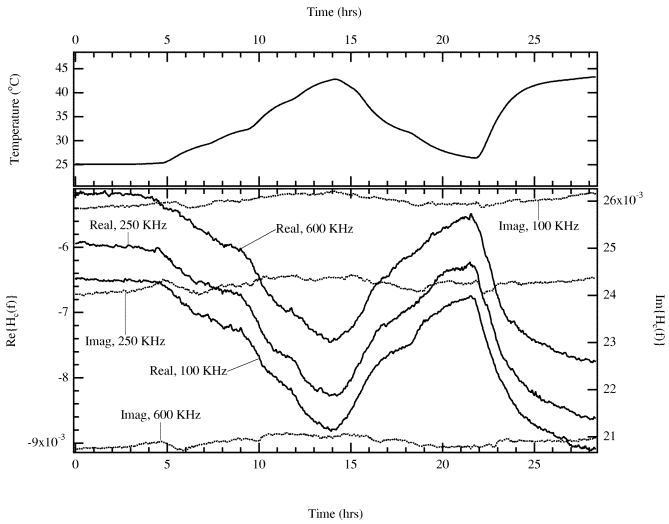

Fig. 6. Variation in $H_c(f)$ with temperature and time.

simple seven-tap complex finite impulse response (FIR) filter (designed using a least squares algorithm [11]) provides less than -70-dBc sideband levels at all frequencies in the band. More than seven taps are required if the sideband levels lower than -70 dBc are desired.

The quadrature modulator is sensitive to ambient conditions, e.g., temperature and carrier frequency. Two approaches exist to ensure that the sideband cancellation filter tracks the quadrature modulator at all times. The obvious approach is to make periodic measurements of the compensator and assume that the compensator is stable between measurements. A second approach is to make the measurements for different ambient conditions and store the compensator in memory. This is the lookup-table approach. Hybrids of these two methods would be commonly used. A good model of the variation of the quadrature modulator with the ambient conditions, e.g., temperature and carrier frequency, is required to make efficient use of memory.

The curves in Fig. 6 show the variation of the real and imaginary parts of $H_c(f)$ at 600, 250, and 100 kHz when the quadrature modulator is subjected to three temperature cycles of 20 °C

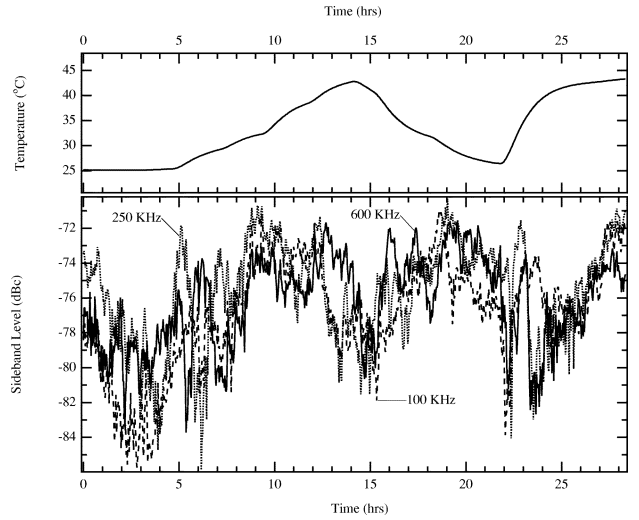

Fig. 7. Sideband attenuation obtained with temperature compensation.

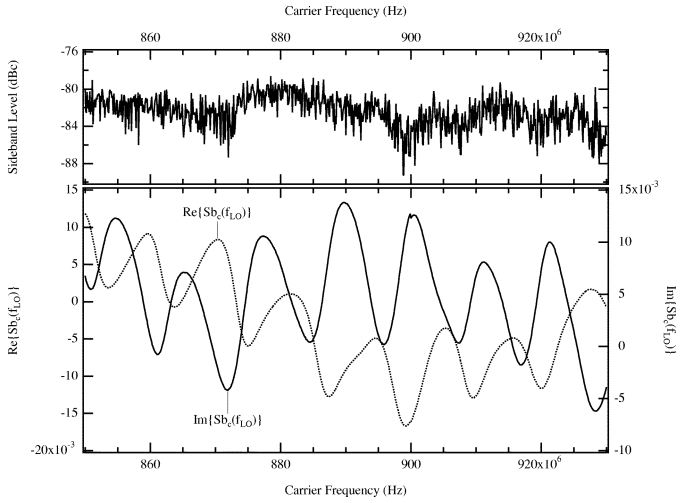

Fig. 8. $\mathrm{Sb}_c(f_{\mathrm{LO}})$ for 850–930 MHz with 100-kHz resolution.

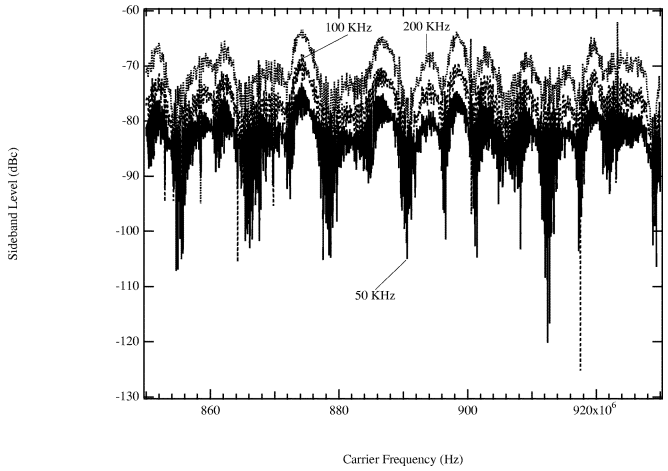

Fig. 9. Sideband attenuation for varying lengths of table look-up.

over a 28-h duration. The data is obtained with the quadrature modulator placed in an oven and the temperature measured on the body of the quadrature modulator. The LO frequency is 850 MHz for this measurement. Two features stand out in the Fig. 6. First, the variation of the filter response at different frequencies is uniform, i.e., the variation of the filter response with temperature corresponds to the proportional variation of a single complex value. This complex value is represented as Sb_c. Second, a gradual drift can be observed in the compensation parameters. (This feature is more distinctly visible in the imaginary part.) Thus, if $H_c(f)$ is the measured sideband cancellation filter at a certain temperature, the filter response at a temperature offset is given by $H_c(f) + \mathrm{Sb}_c$, where $\mathrm{Sb}_c = \text{constant} \times \text{temperature offset} + \text{drift}$. The multiplicative constant has to be determined for each hardware implementation of the quadrature modulator while the offset drift can be removed by periodic measurement of $H_c(f)$ at one frequency point.

Fig. 7 shows that the performance of the temperature-compensated quadrature modulator is better than -70 dBc. The increase from -80 to -70 dBc is due to temperature hysteresis effects in the quadrature modulator, as well as long-term drift. Limited long-term measurements suggest that once a day measurement of $H_c(f)$ at a single frequency with temperature compensation is adequate to get -70 dBc of unwanted sideband level. More long-term data is required to say if there is ever a need to measure $H_c(f)$ at all frequencies after an initial measurement at the time of manufacture.

The sideband cancellation filter $H_c(f)$ depends on the LO frequency, as well as temperature. As with temperature, change in the LO frequency generates a shift in the cancellation filter [3]. This shift, represented by $\mathrm{Sb}_c(f_{\mathrm{LO}})$, depends on the quadrature modulator itself, as well as the constancy of the LO driving impedance, i.e., the synthesizer output. Fig. 8 shows that $\mathrm{Sb}_c(f_{\mathrm{LO}})$ is a well-defined smooth function of f_{LO} over a frequency range of 850–930 MHz. The carrier frequency resolution in this figure is 100 kHz. Fig. 9 shows the attenuation obtained when $\mathrm{Sb}_c(f_{\mathrm{LO}})$ is stored for carrier frequency changes of 200, 100, and 50 kHz, and the nearest stored value is used to obtain the overall cancellation filter. Evaluation of $\mathrm{Sb}_c(f_{\mathrm{LO}})$ for a carrier frequency resolution of 100 kHz is adequate to ensure a sideband level below -70 dBc. Thus, a lookup table combining carrier frequency and temperature can provide -70-dBc sideband levels for approximately a day. For longer periods of time, there has to be some real-time adaptation since there appears to be some nonstationarity in the quadrature modulator properties.

The quadrature modulator is not only intrinsically sensitive to frequency variations, but also to LO drive-level variations. If a sideband level of -70 dBc is required, even small synthesizer imperfections become significant. When the VSA (HP89441a) was used as the LO, a small discontinuity in $\mathrm{Sb}_c(f_{\mathrm{LO}})$ was observed whenever the carrier frequency moved over a 1-MHz scale. This was caused by a 0.1-dB amplitude change produced by the relocking of the coarse phase-locked loop (PLL). This kind of discontinuity is not observed in the data obtained using the HP8862A, which employs a different architecture.

VII. Carrier Compensation

Carrier leakage in most quadrature modulators is specified with respect to the LO input power. In the measurement setup

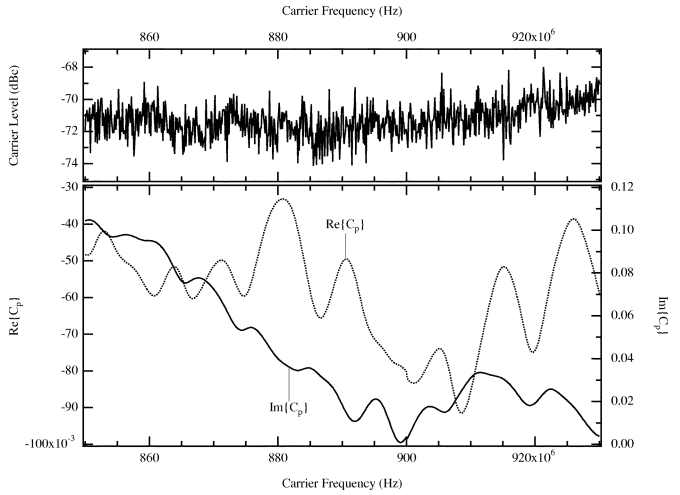

Fig. 10. C_p with varying carrier frequency for 850–930 MHz.

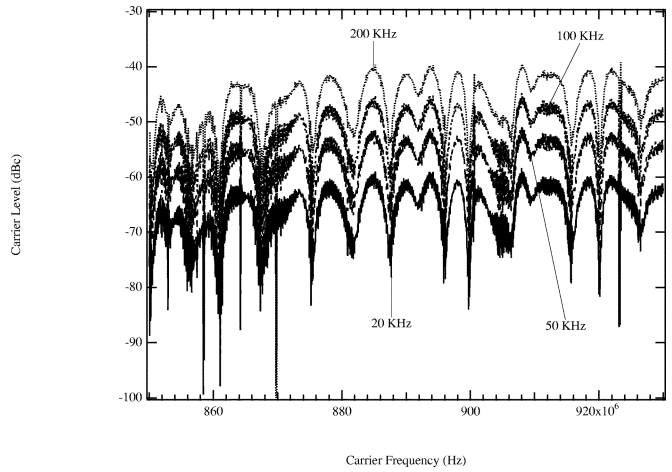

Fig. 11. Carrier attenuation for varying lengths of table look-up.

described here, the LO signal power is 10 dBm and the typical carrier suppression of the raw quadrature modulator is −40 dBc. The signal power at the I and Q phase inputs is chosen to generate low nonlinear distortion in the signal, i.e., second and third harmonic levels lower than −70 dB with respect to the desired signal and, thus, the input to the quadrature modulator is only −39 dBm. Since the desired signal power and the LO leakage at the output of the quadrature modulator are of the same order, effective carrier cancellation is critical.

Fig. 10 shows C_p as carrier frequency varies over 850–930 MHz at a resolution of 100 kHz. The variation of C_p with carrier frequency is far more significant than the variation of Sb_c. Fig. 11 shows the carrier attenuation obtained when $C_p(f_{\mathrm{LO}})$ is stored for carrier frequency steps of 200, 100, 50, and 20 kHz and the carrier-leakage parameter at the closest carrier frequency is used for compensation. A frequency resolution of 10 kHz is required to hold a −70-dBc residual carrier level. On the other hand, more sophisticated interpolation algorithms may be used to reduce the storage requirements since the variation is well defined, as seen in Fig. 10.

Fig. 12 shows the variation of C_p when the quadrature modulator is subjected to four temperature cycles of 10 °C over a 24-h duration. The substantial variation of C_p at the nineteenth hour

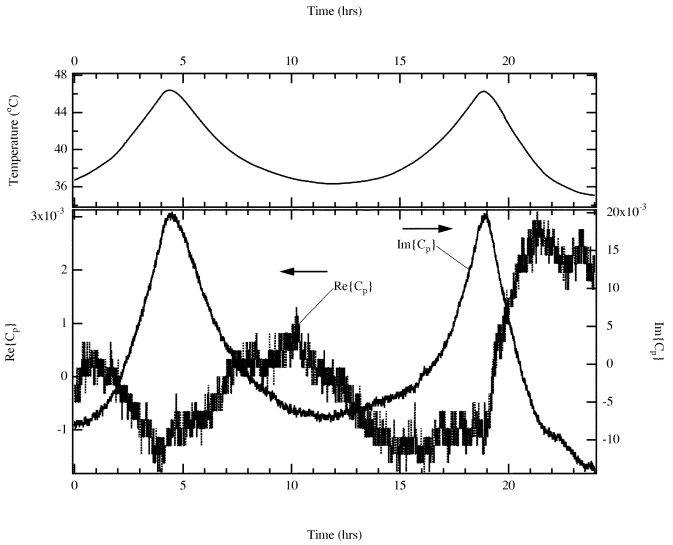

Fig. 12. C_p with varying temperature at 850 MHz.

indicates that the carrier compensation parameter is far more susceptible to drifts in the system than the sideband cancellation parameters. Such nonstationary behavior of the carrier leakage requires real-time adaptation of the compensation parameter to maintain the −70-dBc residual carrier level. However, for moderate time durations (<10 h) the −70-dBc level can be maintained by using simple temperature compensation.

VIII. Summary and Applications

This paper used a low-cost mass-produced quadrature modulator to obtain over 70 dB of spurious-free dynamic range over a 1.2-MHz bandwidth using an extremely low-complexity compensator, e.g., a seven-tap complex FIR filter. The 1.2-MHz bandwidth was set by interference from an induction furnace next door, which introduced significant harmonics upwards of 1.2 MHz. Above 1.2 MHz, the interference was sufficient to spoil the spectrum completely; however, spot frequency measurements showed that the basic approach will work for a bandwidth of 100 MHz with the addition of two more taps. Measurements on the quadrature modulator also show that it can be easily compensated for varying ambient conditions, e.g., temperature and carrier frequency. These modulators have many potential applications.

The most obvious application of very low sideband modulators is to multichannel systems with stringent spurious specifications such as multiuser systems based on frequency-division multiplexing (e.g., analog mobile phone system (AMPS), global system mobile (GSM), FM business radio). To make the transmitter in these systems economical, the signal source generating the RF carrier for the LO should be either fixed tuned or tuned in coarse steps. The fine steps are provided by digital frequency translation within the quadrature modulator's baseband input span. None of these systems employs power control, and most do not allow frequency rearrangement based on user position. Thus, the image sideband usually appears as interference in an adjacent channel and, thus, the image frequency of a nearby user may impinge on the weak signal from a distant user.

Even if baseband tuning is not required, e.g., f_{LO} can be tuned to the center of the RF span, exceptionally low sideband levels are needed if a quadrature modulator must process a nominally constant envelope signal, e.g., an FM voice or continuous phase frequency shift-keying (CPFSK) signal. The image sideband will result in in-band spurious tones that the nonlinear power amplifier following the quadrature modulator will turn into out-of-band spurious emissions. Amplifier linearization using baseband predistortion [8] also requires very high-quality modulators. Such systems sense the distortion produced at the output of the RF amplifier and then correct it by appropriate predistortion of the baseband signal. The overall linearity of the amplifier and modulator system can be made to approach within 10 dB of the quadrature modulator's image sideband level.

REFERENCES

[1] A. A. Abidi, "Direct-conversion radio transceivers for digital communications," *IEEE J. Solid-State Circuits*, vol. 30, pp. 1399–1410, Dec. 1995.

[2] B. Razavi, "Design considerations for direct-conversion receivers," *IEEE Trans. Circuits Syst. II*, vol. 44, pp. 428–435, June 1997.

[3] O. M. Collins and N. Vasudev, "Ultra-linear radio frequency modulators," *IEEE Trans. Commun.*, submitted for publication.

[4] J. Crols and M. Steyaert, "A fully integrated 900 MHz CMOS double quadrature down converter," in *Proc. Int. Solid-State Circuits Conf.*, Feb. 1995, pp. 136–137.

[5] J. Sevenhans *et al.*, "An analog radio front end chip set for a 1.9 GHz mobile radio telephone application," in *Proc. Int. Solid-State Circuits Conf.*, Feb. 1994, pp. 44–45.

[6] M. Faulkner, T. Mattsson, and W. Yates, "Automatic adjustment of quadrature modulators," *Electron. Lett.*, vol. 27, no. 3, pp. 214–216, Jan. 1991.

[7] S. A. Leyonhjelm and M. Faulkner, "The effect of reconstruction filters on direct upconversion in a multichannel environment," *IEEE Trans. Veh. Technol.*, vol. 44, pp. 95–102, Feb. 1995.

[8] A. A. M. Saleh and J. Salz, "Adaptive linearization of power amplifiers in digital radio systems," *Bell Syst. Tech. J.*, vol. 62, no. 4, pp. 1019–1033, Apr. 1983.

[9] O. M. Collins and N. Vasudev, "The effect of redundancy on measurement," *IEEE Trans. Inform. Theory*, vol. 47, pp. 3090–3096, Nov. 2001.

[10] N. Vasudev and O. M. Collins, "Measurement of a filter using a power detector," *IEEE Trans. Microwave Theory Tech.*, vol. 50, pp. 2083–2089, Sept. 2002.

[11] B. Porat, *A Course in Digital Signal Processing*. New York: Wiley, 1997.

N. Vasudev was born in Hyderabad, India. He received the B.E. degree (with honors) in instrumentation from the Birla Institute of Technology and Science, Pilani, India, in 1993, the M.S. degree in electrical engineering from the Indian Institute of Technology, Chennai, India, in 1997, and the Ph.D. degree in electrical engineering from the University of Notre Dame, Notre Dame, IN, in 2001.

He is currently a Design Engineer with Stryker Endoscopy, San Jose, CA. His research interests include communication systems and signal processing.

Oliver M. Collins (S'88–SM'99–F'02) was born in Washington, DC. He received the B.S. degree in engineering and applied science, and the M.S. and Ph.D. degrees in electrical engineering from the California Institute of Technology, Pasadena, in 1986, 1987, and 1989, respectively.

From 1989 to 1995, he was an Assistant Professor and then an Associate Professor with the Department of Electrical and Computer Engineering, Johns Hopkins University, Baltimore, MD. In September 1995, he became an Associate Professor with the Department of Electrical Engineering, University of Notre Dame, Notre Dame, IN. He became a Full Professor in 2001 and currently teaches courses in communications, information theory, coding, and complexity theory.

Dr. Collins was the recipient of the 1994 IEEE Thompson Prize Paper Award, the 1994 Marconi Young Scientist Award presented by the Marconi Foundation, and the 1998 IEEE Judith Resnik Award.